Journal of Materials Chemistry C

Accepted Manuscript

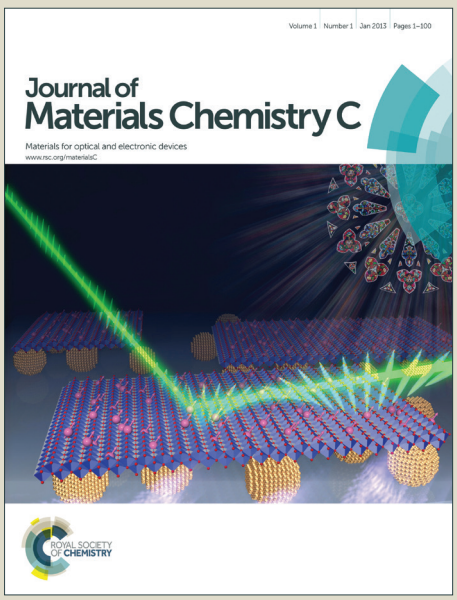

ROYAL SOCIETY OF CHEMISTRY

www.rsc.org/materialsC

Cite this: DOI: 10.1039/c0xx00000x

www.rsc.org/xxxxxx

ARTICLE TYPE

Network assembly of gold nanoparticles linked through fluorenyl dithiol bridge

Maurizio Quintiliani,[a] Mauro Bassetti,[b] Chiara Pasquini,[b] Chiara Battocchio,[c] Marco Rossi,[d,e] Francesco Mura,[d] Roberto Matassa,[e] Laura Fontana,[a] Maria Vittoria Russo,[a] and Ilaria Fratoddi[a,d]*

Received (in XXX, XXX) Xth XXXXXXXXX 20XX, Accepted Xth XXXXXXXXX 20XX
DOI: 10.1039/b000000x

Gold nanoparticles stabilized by two novel bifunctional fluorenyl thiols, generated in situ from 9,9-didodecyl-2,7-bis(acetylthio)fluorene **(1)** and 9,9-didodecyl-2,7-bis(acetylthiophenylethynyl)fluorene **(2)**, exhibit bridged structures which self assemble in parallel lines. The size, shape and structure of the AuNPs has been determined by means of dynamic light scattering (DLS), scanning electron microscopy (FE-SEM), transmission electron microscopy (TEM) and X-ray photoelectron spectroscopy (XPS). AuNPs modified with fluorenyl thiol derivatives show diameters in the range 3 - 7 nm. The linkage between the nanoparticles can be envisaged with the formation of dyads supported by TEM analysis and XPS measurements. Remarkably, investigation by scanning electron microscopy of the AuNPs films revealed an ordered distribution of well-separated individual nanoparticles to form a 2D network. The formation of interconnected networks between AuNPs with different distances, depending on the nature of the thiol linkers **(1)** or **(2)**, and the photoluminescence properties, open perspectives for applications in optical devices and electronics.

Introduction

Gold nanoparticles (AuNPs) elicit an intense research activity because of their peculiar chemical and physical properties. They have been extensively studied for a wide range of applications, ranging from catalysis,[1] chemical and biosensing,[2] nanoelectronics,[3] nonlinear optics,[4] magnetism,[5] biolabelling[6] and cancer nanotheranostics for the combined diagnosis and therapy in medicine.[7]

The control of size, shape and assembling of nanoparticles, on which their optical, electric and catalytic properties depend, represents a challenge in current nanoscience. A convenient approach that allows a control of particle composition, shape and narrow size-distribution consists in functionalization of AuNPs with thiol ligands.[8] Thus, by varying the nature, size of thiol group and Au/S molar ratio it is possible to tailor the optical and electronic properties of AuNPs and to improve their stability. In this context, the research in our group has been recently centered in the stabilization of gold nanoparticles by mono and bi-functional arenethiols,[9] porphyrin-bridged Pd complex,[10] organometallic complexes containing Pt(II) or Pd(II) centers and thiol capped Ag nanoparticles.[11-13]

Fluorene, oligofluorene, and polyfluorene derivatives[14-16] have attracted attention because of their pure blue and efficient electroluminescence that is effective in polymer-based emissive displays, organic light-emitting devices, and solar cells. The chemical structure modification of the fluorene backbone allows to tune their properties.[17] To the best of our knowledge, only few examples of gold nanoparticles stabilized by fluorenyl-alkane-1-thiolates, *i.e.* (9-methyl-9-(8-thiooctyl)-fluorene, 9-(9-fluorenyl)-nonane-1-thiolate and 12-(9-fluorenyl)-dodecane-1-thiolate), have been reported.[18-19]

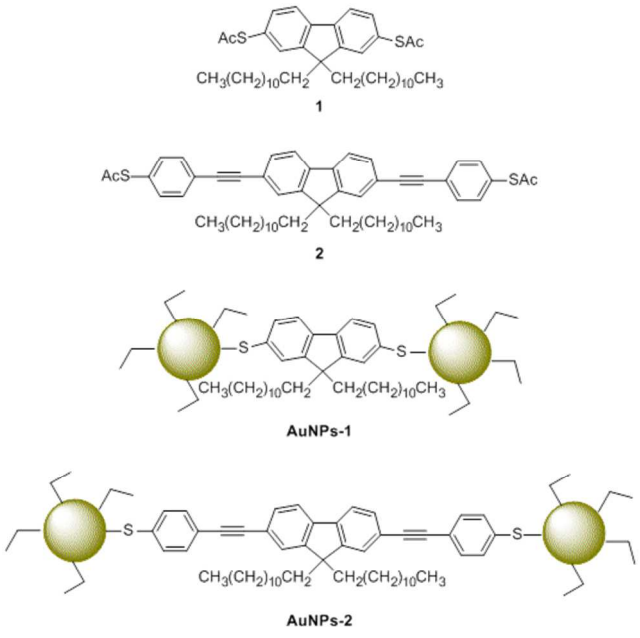

Figure 1: Chemical structure of acetyl protected thiol compounds **(1)** and **(2)** together with **AuNP-1** and **AuNP-2** nanoparticles.

Moreover, self-assembled monolayers (SAM) starting from 2,7-bis(acetylthio)fluorene have been described.[20]

In the present work, 9,9-didodecyl-2,7-bis(acetylthio)fluorene **(1)** and 9,9-didodecyl-2,7-bis(acetylthiophenylethynyl)fluorene **(2)** have been synthesized for the first time and used to stabilize gold nanoparticles. We have varied the conjugation length in between the sulphur donor atoms in order to achieve interconnected networks with different delocalization degree, with the aim to modulate the optical properties. In figure 1, the chemical structure of **AuNP-1** and **AuNP-2** is reported, together with thiolates **(1)** and **(2)**. The size, shape, and structure of these functionalized nanoparticles have been determined by FTIR, UV-vis, NMR, dynamic light scattering (DLS), scanning electron microscopy (FE-SEM), transmission electron microscopy (TEM) and X-ray photoelectron spectroscopy (XPS). A photoluminescence study was carried out to compare the emission properties of the thioesters with those of the corresponding nanoparticles.

Results and Discussion

Synthesis and characterization of ligands.

Fluorenyl bis-thiolacetate **(1)** has been prepared starting from commercially available 9,9-didodecyl-2,7-dibromo-fluorene using a three-step one-pot protocol reported in the literature for the functionalization of 2,7-dibromofluorene and other aromatic dibromides (see SI),[20] in analogy to a dimethyl analog of compound **(1)**, reported in the literature.[21] The nucleophilic aromatic substitution reaction of the two bromine atoms with methylthiolate and in situ transprotection of the resulting methylsulfanyl functional groups provided the terminally thioacetyl-functionalised fluorene **(1)** as a yellow oil in 48% yield.

The synthesis of fluorenyl thiolate **(2)** bearing two ethynylphenyl spacers between fluorene and the terminal thioacetyl groups has been carried out (see SI). The first step consisted in a Sonogashira coupling reaction of 9,9-didodecyl-2,7-dibromofluorene with 2 equivalents of trimethylsilylacetylene (TMSA) to give 1a in 73% yield, according to literature reports for similar compounds,[22-28] followed by deprotection of the triple bonds to give compound **(1b)** in 90% yield. The last step in the synthesis of the target compound **(2)** required the use of 1-(S-acetylthio)-4-iodobenzene, since all attempts to couple **(1b)** with commercially available 4-bromophenylthioacetate failed. 4-Iodo-1-acetylthiobenzene has been obtained by reduction of pipsyl chloride to 1-iodo-4-mercaptobenzene and subsequent treatment in situ with acetyl chloride as reported in the literature.[29-30] Finally, Pd-mediated coupling of the diyne **(1b)** with 4-iodo-1-acetylthiobenzene gave thiolester **(2)** as a yellow oil in 33% yield.

The new compounds **(1)** and **(2)** have been characterized by ^{1}H-NMR, ^{13}C-NMR, FTIR, UV-vis spectroscopy. Elemental analysis are in agreement to the proposed structures, although evidenced the presence of some residual solvent molecules due to the oily compounds. In the ^{1}H-NMR spectra it was possible to observe the peaks corresponding to the acetyl groups (2.4 ppm), the aliphatic chains (0.97-1.84 ppm), the aromatic protons (7.45-7.74), and, for compound **(2)**, the peaks relative to the phenyl groups (7.6 and 7.4 ppm). Similarly, the ^{13}C-NMR spectra presented the peaks corresponding to the acetyl groups (30.2 and 194.2 ppm), and, for compound **(2)**, the peaks relative to the triple bonds (89.0 and 92.1 ppm) and to the phenyl groups. The formation of the final compounds was confirmed also by FTIR spectroscopy, as we observed the presence of the carbonyl band (n = 1712 cm^{-1}), and, for compound **(2)**, the peak assigned to the C≡C triple bonds stretching mode (2199 cm^{-1}).

Synthesis and characterization of gold nanoparticles.

The gold nanoparticles **AuNPs-1**, stabilized with the fluorenyl bis-thiol, in situ obtained from compound **(1)**, were prepared with Au/S molar ratio 1.00/1, 0.70/1, 0.50/1 and 0.25/1 by using a modified Brust's two-phase procedure,[31-33] consisting in a chemical reduction of $HAuCl_4$ in the presence the thiol ligand, $NaBH_4$ as reducing agent and tetraoctylammonium bromide (TOAB) as phase transfer agent (Figure 2). The thioacetyl deprotection occurs and the bifunctional fluorene based thiol is generated during the synthesis.[34]

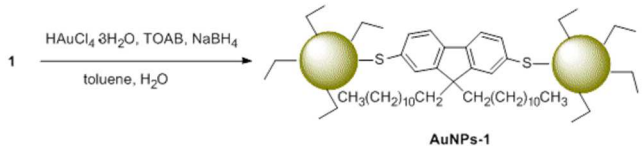

Figure 2: Reaction scheme for the synthesis of **AuNPs-1**

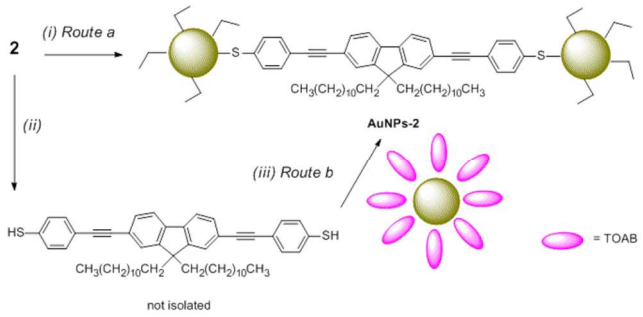

Figure 3: Reaction scheme for **AuNPs-2**. Reagents and conditions: (i) $HAuCl_4 \times 3H_2O$, TOAB, $NaBH_4$, toluene, H_2O, 19°C, 10 min; (ii) NH_4OH 30%, ethanol; (iii) toluene, 25°C, 2 h.

The preparation of **AuNPs-2**, stabilized with thiolate **(2)**, appeared to be very challenging. Following the modified Brust's two-phase procedure (with Au/S molar ratio 1.00/1) according to the standard conditions, we found that gold nanoparticles formed aggregates very quickly and consequently precipitated. For this reason, it was necessary to carry on the reaction at a controlled low temperature (19°C) and to reduce drastically the reaction time to 10 min instead of 2 hours (Figure 3, *route a*). Alternatively, we decided to use a ligand exchange reaction,[35-37] starting from a toluene solution of freshly prepared AuNPs stabilized with tetraocylammonium bromide (AuNPs-TOAB), according to a procedure reported by M. Brust et al.[38] The formation of AuNPs stabilized with TOAB was followed by UV-

vis spectroscopy in toluene, which showed the plasmon absorption peak at 525 nm, characteristic of gold nanoparticles. Subsequent addition of the deacetylated derivative of **(2)**, prepared in situ by treating **(2)** with NH_4OH,[35] afforded AuNPs-2 (Figure 3, *route b*). Comparing the two synthetic pathways, route b resulted to be more advantageous than route a, as it was more effective in the stabilization of the gold nanoparticles and afforded **AuNPs-2** in a higher yield. On the other hand, thiolate **(1)** allowed to obtain more stable gold nanoparticles, while thiolate **(2)** showed an enhanced tendency towards aggregation during the formation of nanoparticles, and this can be attributed to the less distance between the two thiolic moieties in compound **(1)**.

AuNPs-1 were soluble in CH_2Cl_2, $CHCl_3$, toluene and DMF; **AuNPs-2** were soluble only in DMF. All compounds were characterized by spectroscopic techniques (FTIR, UV-vis and NMR). In the FTIR spectra of **AuNPs-1** and **AuNPs-2**, we observed the bands relative to the stretching mode of CH in aliphatic chains (2958, 2933 cm^{-1}) and to the aromatic system CC (1100-600 cm^{-1}), while a weak peak at 1712 cm^{-1}, characteristic of the stretching of carbonyl group, indicate that the deacetylation was not complete and a small percentage of nanoparticles are linked only on one side of the bifuncional thiolate. We could exclude the presence of free thiolates as we accurately washed the solids with ethanol until we couldn't observe the peaks of the starting thiolates in the UV-vis spectra. The FIR spectra showed a band at 226 cm^{-1}, that can be attributed to the stretching Au-S, confirming the formation of gold nanoparticles.[39]

In the ^{1}H-NMR spectra, broad signals corresponding to the aromatic protons (7.7-7.3 ppm) and aliphatic chains (2.1-0.5) were observed, as a consequence of the quadrupole moment of gold;[40] a small peak at 2.44 nm corresponding to the acetyl groups indicated that a small number of nanoparticles are linked only on one side of the bifuncional thiolate, as observed in the FTIR spectra, and this percentage could be calculated as 14% from the ratio between the integrals of this peak and that of the terminal alkyl chain. As a consequence, 86% of the fluorene spacer is covalently bound to the gold surface spanning two nanoparticles.

Optical Properties.

Figure 4 shows the electronic absorption spectra of thiolester **(1)** and nanoparticles **AuNPs-1**. Compound **(1)** presents two narrow peaks at 293 and 317 nm, while AuNPs show a broad peak at 330 with a shoulder at about 300 nm. The presence of the plasmon resonance at about 530 nm confirm the formation of gold nanoparticles. The formation of nanoparticles induces a broadening and a bathochromic shift of 13 nm of the band attributed to the ligand chromophore, while the maximum at about 530 nm corresponds to the plasmon absorption resonance band and confirms the formation of small-sized nanoparticles. The different thiolic ligand content obtained by varying the Au/S molar ratio, does not seem to determine any significant influence in the absorption spectra, since the optical features are overlapping in the different samples.

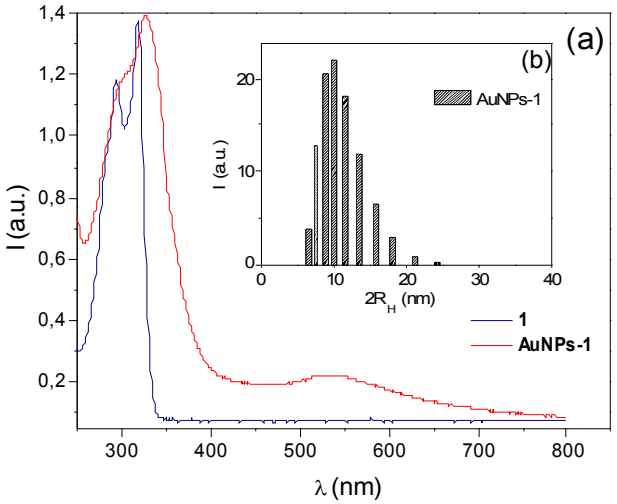

Figure 4: a) UV-vis spectra in CH_2Cl_2 of thiolester **(1)** (blue line) and **AuNPs-1** (red line) with Au/S ratio 1:1; b) DLS data: size distribution in CH_2Cl_2 for **AuNPs-1** with Au/S ratio 1:1 sample.

The size and size-distribution of **AuNPs-1** in organic solutions (CH_2Cl_2) have been investigated by means of DLS measurements. The hydrodynamic data and the average size expressed as $<2R_H>$, gave a size dispersion in the range of 10-18 nm, with a lower diameter obtained by increasing the thiolic ligand content, as expected. In particular, for the 1/1 **AuNPs-1** sample, the mean size was 10 nm. The size distribution consists of a single peak with a narrow size distribution, as shown in Figure 4b for the 1:1, **AuNPs-1** sample.

The electronic absorption spectra of thiolester **(2)** and nanoparticles **AuNPs-2** are depicted in Figure 5. Compound **(2)** exhibits a maximum at 360 nm, that is red-shifted compared to the absorption of thiolester **(1)**, and this bathochromic shift can be attributed to the increase of the π-conjugation. Gold nanoparticles **AuNPs-2** show two peaks at 365 and 593 nm. As in the case of **AuNPs-1**, we observe an enlargement and bathochromic shift of the band attributed to the ligand chromophore. However, the plasmon resonance band is centered at ~593 nm, and we can attribute this value to the cross-linking of particles into network agglomerates.

The hydrodynamic radius of **AuNPs-2** supported the strong tendency to aggregation even in diluite solution, with mean particle size of tens of nm for samples obtained with either *route a* and *route b*. The nanosize was however evidenced by microscopy studies (see next paragraph).

The fluorescence of metal nanoparticles has been the topic of dramatic research efforts.[41] Photoluminescence is an important property and a study was carried out at different excitation wavelengths in order to obtain information on the different contribution to fluorescence that arises from the organic chromophore and chromophore stabilized metal nanoparticles. Then, a comparison of the emission properties of the thioesters **(1)** and **(2)** with those of the corresponding nanoparticles **AuNPs-1** and **AuNPs-2** has been carried out.

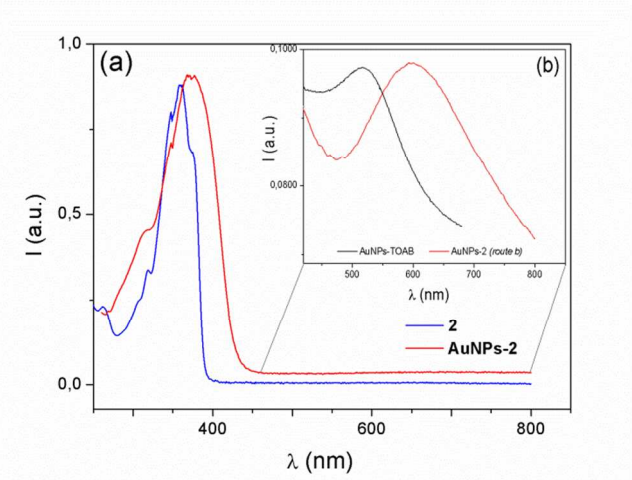

Figure 5: a) UV-vis spectra of thiolester **(2)** (blue line) in CH_2Cl_2 and **AuNPs-2** (purple line) obtained with *route b*, with Au/S ratio 1/1 in DMF; Inset b) Enlargement of the Plasmon band of **AuNPs-2** obtained with *route b* (red line) compared with AuNPs-TOAB (black line).

Figure 6a reports the fluorescence spectra of thiolester **(1)** and nanoparticles **AuNPs-1**. Compound **(1)** shows one peak at 355 nm and a shoulder at 390 nm, while **AuNPs-1** show two peaks at 387 and 409 nm. The formation of nanoparticles induces a bathochromic shift of about 30 nm of the emission band compared to the free ligand.

As reported in the literature, metal nanoparticles have an effect on the fluorescence of chromophores: if the chromophore is in close proximity to the metal surface, its strong electromagnetic field induces a quenching, whereas if the distance increases, typically with long linkers, the fluorescence is enhanced.[42] However, in the case of our thioesters **(1)** and **(2)**, this phenomenon was not evident. The red-shifted emission observed for **AuNPs-1**, with respect to thiolate **(1)**, can be explained considering that the covalent bond formation is accompanied by an electron density flow to the gold center through the S-bridge. As reported in the literature, the charge transfer has an effect on the relative arrangement of energy levels in the AuNP-thiol systems,[43] mainly due to the chemical structure of the thiolate ligand.

In the case of the fluorescence of thiolester **(2)** and nanoparticles **AuNPs-2**, no bathochromic shift was observed moving from the ligand to AuNPs, and both spectra showed two emission bands at around 385 and 405 nm (Figure 6b). This result can be explained considering that as the linker length increases, the distance from the gold core increases and the interaction becomes less effective.[43] The distance between spacer and nanoparticles is not the only parameter that affects the emission properties, conjugation effect should also be taken in account. Emission of gold nanoparticles was also studied, by exciting the samples at the plasmon resonance maxima, respectively at 530 nm for **AuNPs-1** and 580 nm for AuNPs-2. As can be observed in insets of figure 6a and b, emission at about 790 nm is observed for **AuNPs-1** and two peaks are visible for **AuNPs-2** (765 and 820 nm). Considering that as the dimension of the nanoparticle increases the emission wavelength redshifts,[44] in our **AuNPs-2** sample different size populations are probably present.

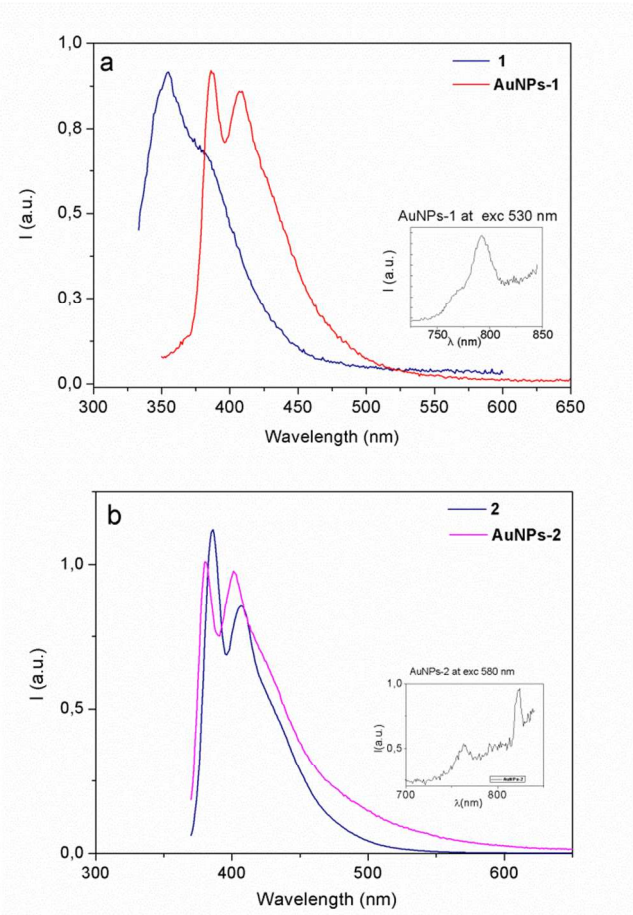

Figure 6: a) Fuorescence spectra of thiolester **(1)** (blue line) in $CHCl_3$ and **AuNPs-1** (red line) with Au/S ratio 0.25/1 in CH_2Cl_2 at λ_{exc} 330 nm. The inset shows the emission spectrum of AuNPs-1 at λ_{exc} 530 nm; b) Fuorescence spectra of thiolester **2** (blue line) in $CHCl_3$ and **AuNPs-2** (purple line) with Au/S ratio 1.00/1 in DMF at λ_{exc} 360 nm. The inset shows the emission spectrum of AuNPs-2 at λ_{exc} 580 nm.

Chemical Structure Study.

XPS measurements were performed on thiolate **(1)**, thiolate **(2)**, **AuNPs-1** (with Au/S = 1/1, 0.25/1 and 0.7/1 stoichiometric ratios), **AuNPs-2** (with Au/S = 1/1 stoichiometric ratio). These measurements aim to detect the degree of linkage between gold nanoparticles and fluorenyl dithiols, *i.e.* whether the ligands always act as bridges between gold nanoparticles or some are attached on one side leaving the ending thiolate group free. For the thiolates the measured C1s, S2p, O1s core level spectra confirm the hypothesized molecular structure (BE values, FWHM and atomic ratios estimated for all thiolates and AuNPs are reported in Table 1 in the Supporting Information). C1s signals are composites for all samples, and by applying a peak-fitting procedure at least three components can be individuated, corresponding respectively to C-C (285.0 eV), C atoms of the thioacetyl group (C-S, COC^*H_3) (about 286.5 eV) and carbonyl groups (C^*OCH_3) (288.0 eV nearly); a fourth component can be observed at higher BE values for fluorenyl-thiolate samples, and is associated to the shake-up peak of the aromatic rings (due to the π-π* transition, at about 292 eV). S2p spectra of thiolates show a single pair of spin-orbit components with the main S2p3/2

feature at 163.5 – 164.0 eV BE, as expected for S atoms in -$SCOCH_3$ groups.[9]

S2p and Au4f signals of AuNPs samples provide useful information about the interaction between the organic thiolate and metallic cluster. Au4f spectra of **AuNPs-1** and **AuNPs-2** are shown in Figure 7; both spectra appear structured, and by following a peak-fitting procedure two pairs of spin-orbit components can be individuated. The first feature (Au4f7/2 BE = 84.0 eV) is associated to metallic gold, and is due to gold atoms in the bulk of nanoparticles.

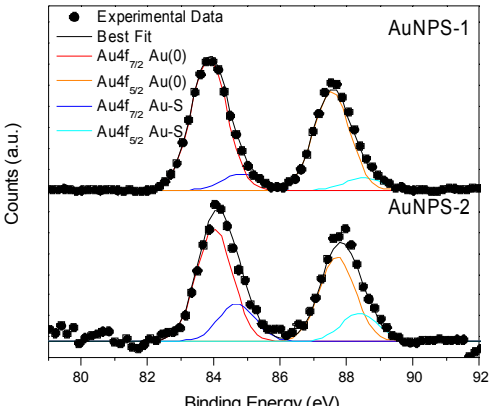

Figure 7: Au4f spectra of **AuNPs-1** and **AuNPs-2**

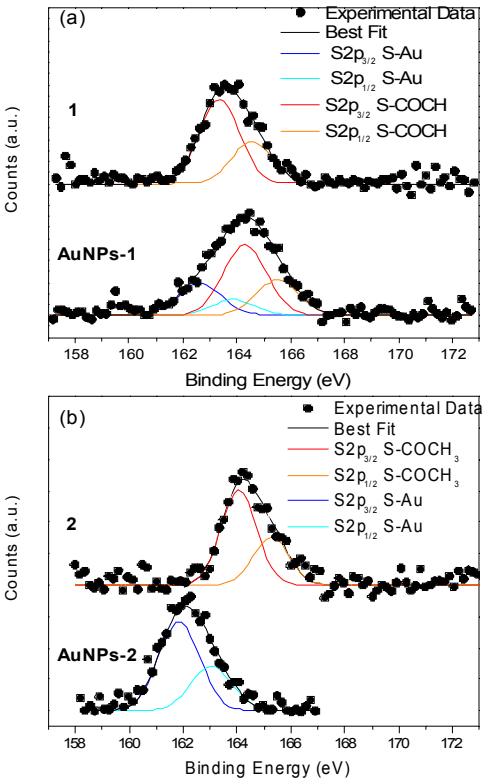

Figure 8: S2p spectra of **AuNPs-1** and **AuNPs-2** compared with thiolates **(1)** and **(2)**

The spin-orbit pair of lower intensity at higher BE values (Au4f7/2 component at nearly 85.0 eV BE) is indicative for positively charged gold atoms, as expected for surface atoms bonded to sulphur. S2p spectra provide complementary information about the chemical bond between thiolates and surface gold atoms of AuNPs. As shown in Figure 8, in AuNPs S2p spectra a new pair of spin-orbit components appears at lower BE values (S2p3/2 BE = 162 eV) (blue line), as expected for sulfur atoms covalently bonded to metals.[12]

In all **AuNPs-1** samples the S2p feature at higher BE values due to free thiolate end-groups is still observable, while in **AuNPs-2** only the signal associated to bonded sulfur atoms can be detected. The atomic ratio between sulfur atoms bonded to gold and free thiolate terminal groups is usually correlated to the mean size of functionalized nanoparticles.[13] In **AuNPs-2**, the presence of a single S2p spin-orbit pair attributed to sulfur atoms covalently bonded to gold, suggest that all thiolate terminal groups are involved in AuNPs functionalization, resulting in a high degree of linkage between nanoparticles.

Morphology and Self-Assembly.

The ability to control the uniformity of the size, shape, composition, and semi-crystalline structure properties of gold nanoparticles topologically connected by two novel bifunctional fluorenyl thiolates is essential for assessing their properties. To obtain insight into the evidence of the local nano-structure of assembling heterobridged gold nanoparticles, a combination of electron microscopy measurements has been applied.

Investigation by scanning electron microscopy at high magnification of the surface of **AuNPs-1** films revealed an array of interacting nanoparticles *i.e.* a network (see Figure 9 a, b and c), showing a uniform distribution of the well-separated functionalized nanoparticles. Accurate observations of SEM images show the presence of NPs morphologically distributed in randomly oriented parallel chains, both straight and curve (see Figure 9 b, c), with a larger Au nanoparticle at the centre that seems to connect two parallel chains. Based on these experimental results, a series of transmission electron microscopy measurements have been performed to study the local organization of functionalized AuNPs network. Image analysis technique has been applied to quantify the dimension of the AuNPs (diameter) and the distance among nearest neighbours of the self-assembled AuNPs. Figure 9d shows a representative bright-field micrographs of **AuNPs-1** exhibiting a two-dimensional network and details are shown in figure 9 e and f.

The AuNPs distributions of a given micrograph have been quantified on probed area of 152 nm by 152 nm, showing a contour map of the AuNPs distribution (see in Figure 9g). The dispersity of the particles size of the **AuNPs-1** compound is clearly visible in the TEM image (see in Figure 9h). **AuNPs-1** have an approximately spherical shape and an average diameter of 5.2 ± 2.0 nm with a polydispersity of 38%. Given the presence of spatially well-separated nanoparticles without overlapping in the bi-dimensional view, it was possible to use a simple method to quantify the distance d_s among the AuNPs.

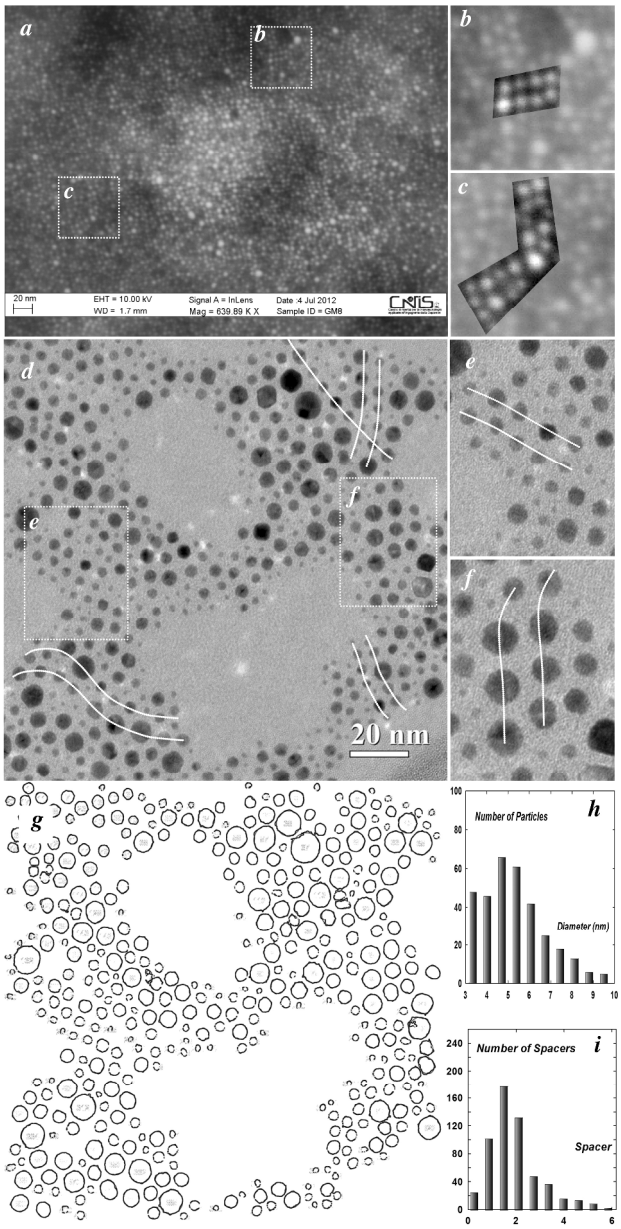

Figure 9: a) High magnification SEM image illustrating the effective order of **AuNPs-1**; b and c) Enlarged images of figure a), evidencing the **AuNPs-1** arranged in network; d) Low-resolution TEM image of **AuNPs-1**; e and f) Details of figure d); g) Processed image of figure d), showing the distribution of 403 gold nanoparticles; h) Plot showing the frequency distribution of the diameters of **AuNPs-1**; i) Distance distribution histogram of **AuNPs-1** nearest neighbours.

To simplify the quantification description, the d_{i-j} distances have been measured between the center of mass of the nearest neighbour nano-objects, minus the corresponding $r_{i,j}$ radius of each AuNP associated to the distance d_{i-j} ($d_s = d_{i-j} - (r_i + r_j)$).[12] In Figure 9i the histogram of the distribution of the calculated distances ds between **AuNPs-1** is shown. The higher-counts value is centered around 1.5 ± 0.3 nm corresponding roughly to the length of the fluorenyl linker,[45] suggesting that about 50% of the NPs are bridged through the organic spacer, in good agreement with XPS results.

AuNPs-2 samples obtained by *route a* and *route b* have been compared by SEM and TEM analysis. In Figure 10 the TEM image together with the quantitative analysis on the distribution of size and distance between **AuNPs-2** obtained with *route a*, is shown.

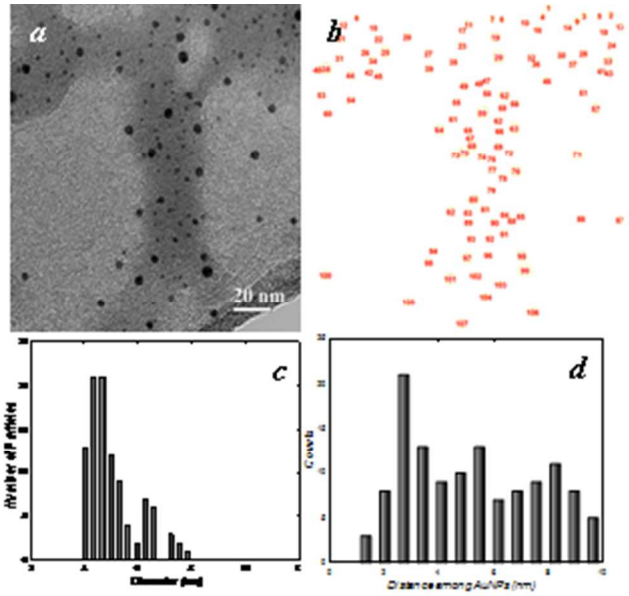

Figure 10: a) Low-resolution TEM image of **AuNPs-2** monolayers separated by thiolate **(2)** obtained by *route a*; b) Processed image showing the distribution of 107 gold nanoparticles, corresponding to the bright field micrograph. c) Plot showing the frequency distribution of the diameters of **AuNPs-2**. d) Distance distribution histogram of AuNPs nearest neighbours.

The histogram in Figure 10c shows an average diameter of the nanoparticles equal to 4.9 ± 1.2 nm with a polydispersity of 25%. The value of the intense peak at about 2.7 ± 0.3 nm (Figure 10d) is in agreement with the calculated length of the fluorenyl spacer **(2)**. The next main counts are distributed around 5.5 ± 0.4 nm and 8.2 ± 0.4 nm, which can be related to the parallel non-covalent interactions among fluorenyl bridges of two nearest stabilized AuNPs. These d_s values can be consistent with the distance between the head-tail of sulphur atoms of two aligned separated complexes.[12]

SEM and TEM images of **AuNPs-2** obtained by *route b* are shown in Figure 11. High magnification study of **AuNPs-2** revealed also in this case a network of interconnected nanoparticles (see Figure 11 a, b and c), showing well-separated nanoparticles that self assembly in almost parallel chains, more distanced with respect to the **AuNPs-1** (see SEM images in Figure 9). A TEM bright field image of **AuNPs-2** obtained by route b is shown in Figure 11e. As it can be observed, aggregates in a 3D network are present, probably due to the high degree of bridging between NPs, as XPS data suggested.

This avoided the visualization of well isolated NPs and it did not allow us to rule out the statistical image of TEM analysis. The corresponding high magnification shown in Figure 11f evidences an overlapping of the quasi-spherical shape gold nanoparticles with a diameter of about 5 nm.

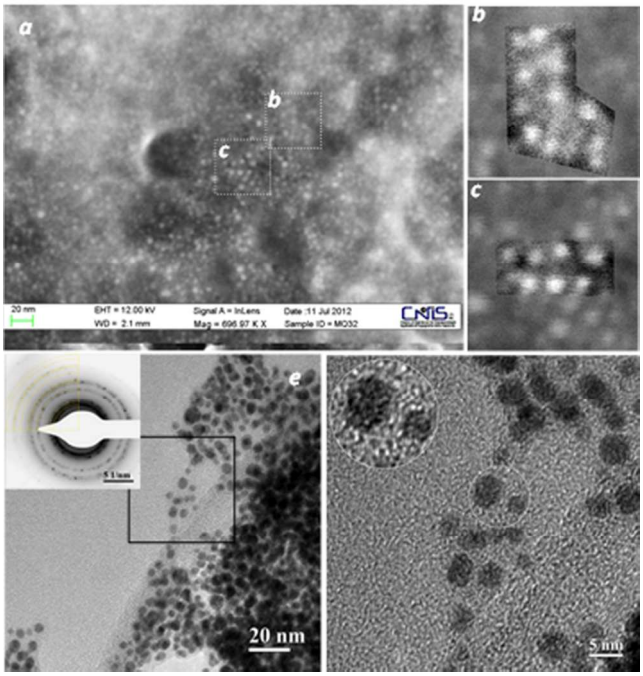

Figure 11: a) High magnification SEM image illustrating the effective ordered of **AuNPs-2** obtained by route b; b and c) Enlarged images of figure a) evidence the **AuNPs-2** arranged in network. e) Low-resolution TEM image of poly-dispersed AuNPs aggregation separated by complex bridged. Inset: Corresponding diffraction pattern of figure 3a) shows distinct diffraction spots or rings for each of the face-centered-cubic Au phase. f) High magnification image showing the multilayers of **AuNPs-2**, inset showing the gold lattice fringes.

The inset is a representative enlarged image of white circle area showing the lattice fringes of the Au nanoparticles having interplanar spacing of d_{111} = 0.238 nm. In order to confirm the crystallographic fingerprint of the atomic species, the electron diffraction pattern (EDP) (Inset of Figure 11e) have been performed showing the typical pattern of face-centered-cubic (fcc) gold crystal of space group Fm-3m (yellow arcs). EDP analysis reveals the presence of concentric diffractions rings generated by the different crystallographic orientations of the NPs respect to the electron beam direction. The experimental intensive inner ring corresponds to the typical diffraction ring of Au with interplanar spacing of d_{111} = 0.236 nm.

Conclusion

In conclusion, two series of gold nanoparticles stabilized by two novel bifunctional thiol derivatives of 9,9-didodecyl-2,7-dibromofluorene with a different degree of conjunctional length, **AuNPs-1** and **AuNPs-2**, have been synthesised. The size control of the Au nanoparticles was achieved by careful control of the synthesis parameters. UV-vis spectroscopy evidenced the plasmon resonance for **AuNPs-1** at about 530 nm, whereas in the case of **AuNPs-2** it was found at about 593 nm, suggesting the formation of aggregated structures. The band attributed to the ligand chromophore exhibited a bathochromic shift with respect to that of the free thiolate ligands and was observed at 330 and 365 nm for **AuNPs-1** and **AuNPs-2**, respectively. The emission spectroscopy evidenced a red shift of about 30 nm of the emission band for nanoparticles **AuNPs-1**, that show two peaks at 387 and 409 nm, compared to the free thioester **(1)**, suggesting an electron density flow to the gold center through the S-bridge. This effect was quenched in **AuNPs-2**, that shows two emission bands at around 385 and 405 nm, probably due to the increased distance of the fluorenyl chromophore from the gold core. S2p and Au4f XPS signals of AuNPs samples provide useful information about the interaction between the organic thiolate and nanoparticle. Au4f spectra allowed to isolate the components arising

from metallic bulk gold atoms from those due to surface atoms bonded to sulphur. S2p spectra provide complementary information about the chemical bond; sulfur atoms are mainly covalently bonded to gold surfaces. In **AuNPs-1** samples few free thiolate end-groups are still observable, while in **AuNPs-2** only the signal associated to bonded sulfur atoms can be detected. In **AuNPs-2** all thiolate terminal groups are involved in the covalent bonding, resulting in a high degree of linkage between nanoparticles. Investigation by FESEM and TEM of the surface of **AuNPs-1** films revealed an array of interacting nanoparticles *i.e.* a network showing a uniform distribution of the well-separated functionalized nanoparticles with approximately spherical shape and an average diameter of 5.2 ± 2.0 nm with a polydispersity of 38%. The distance between neighbour nanoparticles of 1.5 ± 0.3 nm is in agreement with the formation of NPs bridged through the organic fluorenyl spacer. **AuNPs-2** nanoparticles showed an average diameter equal to 4.9 ± 1.2 nm with a polydispersity of 25%. A network of interconnected, well-separated nanoparticles, more distanced with respect to the **AuNPs-1** was observed. The bifuncional fluorenyl thiolates induce the self assembly of a network architecture with a uniform distribution, which makes these materials promising candidates in the field of optical devices and electronics.

Experimental Section

^{1}H-NMR and ^{13}C-NMR spectra were recorded on a Bruker Avance II 300 instrument with $CDCl_3$ solvent peaks as reference. FTIR spectra have been recorded as films deposited by casting from CH_2Cl_2 solutions using KRS-5 cells, with a Bruker Vertex 70 spectrophotometer. UV-vis spectra were run in $CHCl_3$, CH_2Cl_2 or DMF solution by using quartz cells with a Varian Cary 100 Scan UV-vis spectrophotometer. The molar extinction coefficients (ε,$M^{-1}cm^{-1}$) were measured in the concentration range of $5.0 \times 10^{-6} \sim 1.8 \times 10^{-4}$ M, and the values are given with ± 5% experimental error. Photoluminescence measurements were carried out on a Horiba Jobin Yvon Fluoromax-4 instrument, on freshly prepared solutions in $CHCl_3$, CH_2Cl_2 or DMF solvents, in the concentration range of 10^{-6} M. Elemental Analyses have been carried out on an EA 1110 CHNS-O instrument. Size and size distribution of AuNPs in CH_2Cl_2 or DMF solution have been investigated by means of dynamic light scattering (DLS) technique by using a Brookhaven instrument (Brookhaven, NY) equipped with a 10 mW HeNe laser at a 632.8 nm wavelength at a temperature of (25.0 ± 0.2)°C. Correlation data have been acquired and fitted in analogy to our previous work.[46] X ray photoelectron (XPS) spectra were recorded using a custom

designed spectrometer, described in a previous work.[13] and equipped with a non monochromatized Mg Kα X-rays source (1253.6 eV Pass Energy = 25 eV, step 0.1 eV). The spectra have been acquired on films casted or spin deposited from $CHCl_3$, CH_2Cl_2 or DMF solvents on TiO_2/Si (111) wafers. The spectra were energy referenced to the C1s signal of aliphatic C atoms having a binding energy BE = 285.00 eV. Atomic ratios were calculated from peak intensities using Scofield's cross section values and λ factors were used.[47] Curve-fitting analysis of C1s, S2p and Au4f spectra was performed using Gaussian profiles as fitting functions, after subtraction of a Shirley-type background. For quantitative data, the BE values were referred to NIST data.[48] Transmission electron microscopy measurements were carried out using a FEI-TITAN TEM operating at 80 kV. Measurements were carried out using the same experimental setup of the previously reported structural studies.[12] on cast deposited samples obtained from CH_2Cl_2 or DMF solutions on Cu grids coated with amorphous carbon. FE-SEM images have been acquired with the Auriga Zeiss instrument (resolution 1 nm, applied voltage 6-12 kV) on freshly prepared films drop casted from CH_2Cl_2 or DMF solution on a metallic sample holder.

Materials and Methods

9,9 didodecil-2,7-dibromofluorene, 1,3-dimetil-2-imidiazolinone (DMI); sodium methanthiolate, acetyl chloride, CuI, Zn powder, trimethylsilylacetylene, K_2CO_3, $Pd(dba)_2$, PPh_3, $[Pd(PPh_3)_2Cl_2]$, tetrachloroauric(III) acid triidrate ($HAuCl_4 \cdot 3H_2O$) tetraoctylammonium bromide (TOAB), sodium borohydride ($NaBH_4$), have been used as received (Aldrich reagent grade). Anhydrous solvents: toluene, THF, CH_2Cl_2, DMF, MeOH, $CHCl_3$, diisopropylamine, diisopropylethylamine (DIEA) (Aldrich reagent grade) have been used as received. Column chromatography was carried out on silica gel Merck (70-230 mesh), and thin-layer chromatography (TLC) on aluminium sheets precoated with silica gel 60 F254 (Merck). Deionized water, obtained from Zeener Power I Scholar-UV (18.2 MΩ), was degassed for 30 minutes with Argon, before use. 4-Iodo-1-acetylthiobenzene was prepared according to procedures reported in the literature.[29-30]

9,9-didodecyl-2,7-bis(acetylthio)fluorene (1)

9,9-didodecyl-2,7-dibromo-fluorene (1.001 g, 1.51 mmol) was dissolved in dry, Ar-saturated DMI (30 mL) and the mixture was heated to 120°C. Sodium methanthiolate (1.015 g, 14.49 mmol) was added at once. The reaction was kept at this temperature for 18 h and then cooled to room temperature. After addition of acetyl chloride (1 mL, 1.104 g, 14.06 mmol) the solution was stirred at room temperature for 3 h and then poured on ice/water. The aqueous phase was extracted with toluene, the organic extracts were dried over Na_2SO_4 and the solvent removed by rotary evaporation. The dark oily product was purified by column chromatography (silica gel, petroleum ether/ CH_2Cl_2 with gradient from 3/1 to 2/1) affording **(1)** as a yellow oil (0.470 g, 48%), R_f = 0.14 (petroleum ether/CH_2Cl_2 3/1). ^{1}H-NMR ($CDCl_3$, 300 MHz): d 7.74 (dd, J = 7.5, 1.0 Hz, 2H, H-4, H-5), 7.45-7.35 (m, 4H, H-3, H-6, H-1, H-8), 2.44 (s, 6H, $COCH_3$), 2.07-1.84 (m, 4H, $CH_2(CH_2)_9$), 1.41-0.97 (m, 36H, $(CH_2)_9$), 0.97-0.80 (m, 6H, CH_2CH_3), 0.80-0.53 (m, 4H, CH_2CH_3). 13C-NMR ($CDCl_3$, 75.5 MHz): d 14.11 (CH_2CH_3), 22.67, 23.75, 29.20, 29.32, 29.53, 29.55, 29.60, 29.94 (CH_2), 30.19 ($COCH_3$), 31.89, 39.98 (CH_2), 55.49 (C-9), 120.68, 127.01, 129.03, 133.11, 141.32, 151.89 (Ar), 194.16 ($COCH_3$). FT-IR (film, ν, cm^{-1}): 2926, 2854, 1712 (C=O), 1462, 1454, 1403, 1352, 1259, 1123, 1006, 948, 886, 815, 754, 723, 614. UV-vis ($CHCl_3$), λ_{max} (nm) (log ε_o): 317 (4.4), 293 (4.3). Elemental analysis calcd. (%) for $C_{41}H_{62}O_2S_2$ (651.06): C 75.64, H 9.60, S 9.85; found: C 74.44, H 9.41, S 10.06.

9,9-didodecyl-2,7-bis(trimethylsilylethynyl)fluorene (1a)

Air was removed from a solution of 9,9-didodecyl-2,7-dibromo-fluorene (2.094 g, 3.17 mmol), CuI (0.082 g, 0.43 mmol), and $[Pd(PPh_3)Cl_2]$ (0.223 g, 0.3177 mmol) in anhydrous diisopropylamine (30 mL) by blowing Ar. Then trimethylsilylacetilene (1.35 mL, 0.938 g, 9.55 mmol) was slowly added at room temperature. The solution turned red at once and then changed to deep brown. The mixture was stirred at 75°C overnight. The solvent was evaporated to dryness, the residue redissolved in Et_2O (50 mL) and the solution washed with diluite HCl (2 x 50 mL) followed by water (2 x 50 mL). Upon filtration though a pad of celite, the filtrate was treated with saturated $NaHCO_3$ (2 x 50 mL) and water (2 x 50 mL) and the organic phase dried over Na_2SO_4. The dark oily product was purified by column chromatography (silica gel, petroleum ether) affording **(1a)** as a yellow oil that solidified at -20°C (1.621 g, 73%), R_f = 0.18 (petroleum ether). ^{1}H-NMR ($CDCl_3$, 300 MHz): d 7.60 (dd, J = 7.8, 0.6 Hz, 2H, H-4, H-5), 7.47 (dd, J = 7.8, 1.4 Hz, 2H, H-3, H-6), 7.43 (dd, J = 1.3, 0.6 Hz, 2H, H-1, H-8), 2.02-1.88 (m, 4H, $CH_2(CH_2)_9$), 1.36-0.95 (m, 36H, $(CH_2)_9$), 0.95-0.81 (m, 6H, CH_2CH_3), 0.61-0.46 (m, 4H, CH_2CH_3), 0.30 (s, 18H, $Si(CH_3)_3$). ^{13}C-NMR ($CDCl_3$, 75.5 MHz): d 0.04 ($Si(CH_3)_3$), 14.12 (CH_2CH_3), 22.68, 23.66, 29.32, 29.55, 29.59, 30.03, 31.90, 40.37 (CH_2), 55.21 (C-9), 94.22 (C≡CSi), 106.09 (C≡CAr), 119.80, 121.75, 126.20, 131.21, 140.83, 150.91 (Ar). FT-IR (film, ν, cm^{-1}): 2957, 2926, 2854, 2154 (C≡C), 1464, 1421, 1377, 1331, 1249, 1216, 1130, 1104, 844, 759, 721, 699, 647. UV-vis ($CHCl_3$), λ_{max} (nm) (log ε_o): 341 (5.0), 326 (4.8), 308 (4.7).

9,9-didodecyl-2,7-diethynylfluorene (1b)

9,9-Didodecyl-2,7-bis(trimethylsilylethynyl)fluorene **(1a)** (0.502 g, 0.72 mmol) was dissolved in Et_2O (13 mL) to give a colorless solution and a catalytic amount of K2CO3 (0.105 g, 0.76 mmol) in MeOH (13 mL) was added. A milky solution was obtained after 24 h at room temperature. The solvent was removed and the crude product was purified by column chromatography (silica gel, petroleum ether) to afford a yellow solid **(1b)** (0.360 g, 90%), R_f = 0.34 (petroleum ether). ^{1}H-NMR ($CDCl_3$, 300 MHz): d 7.64 (dd, J = 7.7, 0.9 Hz, 2H, H-4, H-5), 7.53-7.46 (m, 4H, H-3, H-6, H-1, H-8), 3.16 (s, C≡CH, 2H), 2.02-1.87 (m, 4H, $CH_2(CH_2)_9$), 1.36-0.97 (m, 36H, $(CH_2)_9$), 0.95-0.81 (m, 6H, CH_2CH_3), 0.68-0.49 (m, 4H, CH_2CH_3). ^{13}C-NMR ($CDCl_3$, 75.5 MHz): d 14.11 (CH_2CH_3), 22.67, 23.66, 29.24, 29.32, 29.54, 29.59, 29.94, 31.89, 40.20 (CH_2), 55.19 (C-9), 77.32 (C≡CH), 84.51 (HC≡CAr), 119.94, 120.84, 126.53, 131.23, 140.96, 151.03 (Ar). FT-IR (film, ν, cm^{-1}): 3311 (C≡H), 2926, 2854, 2107 (C≡C), 1464, 1415, 1377, 1200, 891, 823, 755, 721, 648, 605. UV-vis ($CHCl_3$),

λ_{max} (nm) (log ε_o): 330 (4.8), 316 (4.5), 302 (4.6). Elemental analysis calcd. (%) for $C_{41}H_{58}$ (550.90): C 89.39, H 10.61; found: C 89.94, H 10.68.

9,9-didodecyl-2,7-bis(acetylthio phenyl ethynyl)fluorene (2)

Air was removed from a solution of 9,9-didodecyl-2,7-diethynyl-fluorene **(1b)** (0.559 g, 1.015 mmol), 4-iodo-1-thioacetylbenzene (0.847 g, 3.047 mmol), $Pd(dba)_2$ (0.042 g, 0.0725 mmol), CuI (0.027 g, 0.1428 mmol), and PPh_3 (0.076 g, 0.2904 mmol) in anhydrous tetrahydrofuran (16 mL) and anhydrous diisopropylethylamine (1.5 mL) by blowing Ar. The mixture was stirred at 50°C during 24 h. Upon filtration though a pad of celite, the solvent was evaporated to dryness. The dark oily product was purified by column chromatography (silica gel, petroleum ether/ CH_2Cl_2 with gradient from 3/1 to 2/1) affording **(2)** as a yellow oil (0.269 g, 33%), R_f = 0.34 (petroleum ether/CH_2Cl_2 2/1). ^{1}H-NMR ($CDCl_3$, 300 MHz): d 7.69 (d, J = 7.7 Hz, 2H, H-4, H-5), 7.60 (m, J_{AX} = 8.4 Hz, 4H, AA'XX' Ar), 7.56-7.50 (m, 4H, H-3, H-6, H-1, H-8), 7.42 (m, J_{AX} = 8.3 Hz, 4H, AA'XX' Ar), 2.45 (s, 6H, $COCH_3$), 2.07-1.92 (m, 4H, $CH_2(CH_2)_9$), 1.38-0.97 (m, 36H, $(CH_2)_9$), 0.94-0.79 (m, 6H, CH_2CH_3), 0.71-0.52 (m, 4H, CH_2CH_3). ^{13}C-NMR ($CDCl_3$, 75.5 MHz): d 14.09 (CH_2CH_3), 22.65, 23.72, 29.29, 29.54, 29.58, 29.68 (CH_2), 30.00, 30.27 ($COCH_3$), 31.87, 40.32 (CH_2), 55.28 (C-9), 89.01 (C≡C), 92.09 (C≡C), 120.03, 121.62, 124.61, 126.01, 127.96, 130.87, 132.06, 132.11, 132.13, 134.16, 134.21, 134.23, 140.87, 151.16 (Ar), 193.48 ($COCH_3$). FT-IR (film, ν, cm^{-1}): 2925, 2853, 2216, 2199 (C≡C), 1905, 1714 (C=O), 1591, 1490, 1464, 1417, 1397, 1377, 1352, 1289, 1264, 1122, 1016, 949, 890, 826, 739, 623, 605, 544. UV-vis ($CHCl_3$), λ_{max} (nm) (log ε_o): 360 (4.9). Elemental analysis calcd. (%) for $C_{57}H_{70}O_2S_2$ (851.29): C 80.42, H 8.29, S 7.53; found: C 78.92, H 8.36, S 7.82.

Synthesis of gold nanoparticles stabilized with the thiol ligands generated in situ from the acetyl derivative (1) (AuNPs-1)

Gold nanoparticles were prepared by mixing $HAuCl_4 \times 3H_2O$ and compound **(1)** with Au/S molar ratios 1.00/1, 0.70/1, 0.50/1 and 0.25/1. One of these syntheses (Au/S = 1.00/1) is reported as a typical procedure: an aqueous solution of $HAuCl_4 \times 3H_2O$ (0.050 g, 0.128 mmol) in deionized water (4 mL), was mixed with a solution of tetraoctylammonium bromide (TOAB) (0.083 g, 0.152 mmol) in toluene (9 mL). The two-phase mixture was vigorously stirred until all the tetrachloroaurate was transferred into the organic layer and a solution of thiolester **(1)** (0.040 g, 0.062 mmol) in toluene (9 mL) was then added. A freshly prepared aqueous solution of sodium borohydride (0.047 g, 1.271 mmol) in deionized water (4 mL) was rapidly added with vigorous stirring. After further stirring for 3 h, the organic phase was separated, washed with water, and then reduced to 2 mL in a rotary evaporator. After addition of 40 mL of ethanol, the mixture was kept overnight at -18°C and then centrifuged at 1500 rpm for 15 min. The supernatant, containing excess thiol and TOAB, was separated and the precipitate was washed by centrifugation with ethanol in the same way for other 10 times. After removal of the supernatant, a red ruby solution of **AuNPs-1** nanoparticles was then prepared taking up with 10 mL of toluene; the yield was 40% wt. Elemental analysis (%): C 39.97, H 5.18, S 5.50. UV-vis ($CHCl_3$), λ_{max} (nm): 330, 530.

Synthesis of gold nanoparticles stabilized with the thiol ligands generated in situ from the acetyl derivative (2) (AuNPs-2)

AuNPs-2 have been prepared by means of the above described method (*route a*) and by means of ligand exchange procedure (*route b*). In *route a*, **AuNPs-2** gold nanoparticles stabilized with the thiolate derived from **(2)** were prepared by reduction of $HAuCl_4 \cdot 3H_2O$ with $NaBH_4$ in the presence of thiolester **(2)**, as described above, with Au/S molar ratios 1.00/1. However, to prevent aggregation, it was necessary to carry out the reaction at 19°C and to stop stirring just 10 minutes after the addition of sodium borohydride.

By using *route b*, the preparation of **AuNPs-2** has been achieved in a two steps way. In a first step, the preparation of a toluene solution of gold nanoparticles stabilized with TOAB has been carried out as follows. An aqueous solution of $HAuCl_4 \cdot 3H_2O$ (0.046 g, 0.117 mmol) in deionized water (3.9 mL) was mixed with a solution of TOAB (0.284 g, 0.52 mmol) in toluene (10.4 mL) and vigorously stirred until all the tetrachloroaurate was transferred into the organic layer. A freshly prepared aqueous solution of sodium borohydride (0.055 g, 1.46 mmol) in deionized water (3 mL) was rapidly added with vigorous stirring. After further stirring for 2 h the ruby-coloured organic phase was separated and washed once with aqueous sulfuric acid (0.1 M) to remove excess $NaBH_4$, washed twice with aqueous sodium carbonate (1 M), and washed 5 times with water. Yield 18% wt.

In the latter step, the freshly prepared AuNPs in toluene solution have been stabilized in a ligand exchange procedure with **(2)**, as follows. To a solution of compound **(2)** (0.050 g, 0.058 mmol) in ethanol (10 mL), NH_4OH 30% (150 μL) was added and the resulting mixture was stirred vigorously during 10 min. This mixture was added to the toluene solution of gold nanoparticles stabilized with TOAB previously prepared. After further stirring for 2 h, the volume of the solvent was reduced to 2 mL in a rotary evaporator, and 40 mL of ethanol were added. The mixture was kept overnight at -18°C and then centrifuged at 1500 rpm for 15 min to remove the excess of thiol and TOAB. The supernatant was separated and the precipitate was washed by centrifugation with ethanol, and then with dichloromethane for other 10 times. After the removal of the supernatant, a dark solution of AuNP nanoparticles was then prepared by taking up with 10 mL of DMF. The yield was 20% wt. Elemental analysis (%): C 27.40, H 2.73, S 2.73. UV-vis ($CHCl_3$), λ_{max} (nm): 365, 593.

Acknowledgements

The authors acknowledge for financial support Ateneo Sapienza 2011/C26A11PKS2. This work has been partially supported by the Dipartimento di Chimica, Sapienza Università di Roma through the Supporting Reseach Initiative 2013. This Part of the work was carried out with the support of the European Community. We appreciate the support of the European Research Infrastructure EUMINAfab (funded under the FP7 specific

programme Capacities, Grant Agreement Number 226460) and the Advanced Microscopy Laboratory (AML) in CRANN for the provision of their facility and expertise.

Notes and references

[a] Dr. M. Quintiliani, Dr, L. Fontana, Prof. M. V. Russo, and Dr. I. Fratoddi, Department of Chemistry University of Rome Sapienza P.le A. Moro 5, 00185, Rome Italy E-mail: ilaria.fratoddi@uniroma1.it
[b] Dr. M. Bassetti, Dr. C. Pasquini, CNR, Istituto di Metodologie Chimiche, Sezione Meccanismi di Reazione, Dipartimento di Progettazione Molecolare, P.le A. Moro 5, 00185 Rome Italy
[c] Dr. C. Battocchio, Department of Physics, Unità INSTM and CISDiC University Roma Tre, Via della Vasca Navale 85, 00146 Rome, Italy
[d] Dr. F. Mura, Center for Nanotechnology for Engineering (CNIS) University of Rome Sapienza P.le A. Moro 5, 00185 Rome, Italy
[e] Prof. M. Rossi, Dr. R. Matassa Department Fundamental and Applied Sciences for Engineering, University of Rome Sapienza Via Antonio Scarpa 14, 00161 Roma, Italy
† Electronic Supplementary Information (ESI) available: reaction schemes, main spectroscopic characterizations and tables. See DOI:10.1039/b000000x/

References

[1] Mikami, Y.; Dhakshinamoorthy, A.; Alvaro, M.; García, H. *Catalysis Science and Technology* **2013**, 3, 58-69.
[2] Saha, K.; Agasti, S.S. ; Kim, C.; Li, X.; Rotello, V.M. *Chem. Rev*. **2012**, 112, 2739-2779.
[3] Han, S.-T.; Zhou, Y.;Xu, Z.-X.; Huang, L.-B.; Yang, X.-B.;Roy, V.A.L. *Adv. Mater*., **2012**, 24, 3556-3561.
[4] Philip, R.; Chantharasupawong, P.; Qian, H.; Jin, R.; Thomas, J. *Nano Letters* **2012**, 12, 4661-4667.
[5] Nealon, G.L.; Donnio, B.; Greget, R.; Kappler, J.-P.; Terazzi, E.; Gallani, J.-L. *Nanoscale,* **2012**, 4, 5244-5258
[6] Bastús, N.G.; Sánchez-Tilló, E.; Pujals, S.; Farrera, C.; López, C.; Giralt, E.; Celada, A.; Lloberas, J.; Puntes, V. F. *ACS Nano* **2009**, 3, 1335-1344.
[7] Shi, Y., Goodisman, J.; Dabrowiak, J.C. *Inorg. Chem*., **2013**, 52, 9418–9426.
[8] Daniel, M.C.; Astruc, D. *Chem. Rev*. **2004**, 104, 293-346.
[9] Fratoddi, I.; Venditti, I.; Battocchio, C.; Polzonetti, G.; Bondino, F.; Malvestuto, M.; Piscopiello, E.; Tapfer, L.; Russo, M.V. *J. Phys. Chem. C* **2011**, 115, 15198-15204.
[10] Fratoddi, I.; Battocchio, C.; Polzonetti, G.; Sciubba, F.; Delfini, M.; Russo, M.V. *Eur. J. Inorg. Chem.* **2011**, 31, 4906-4913.
[11] Vitale, F.; Vitaliano, R.; Battocchio, C.; Fratoddi, I.; Giannini, C.; Piscopiello, E.; Guagliardi, A.; Cervellino, A.; Polzonetti, G.; Russo, M. V.; Tapfer, L. *Nanoscale Research Letters* **2008**, 3, 461-467.
[12] Matassa, R.; Fratoddi, I.; Rossi, M.; Battocchio, C.; Caminiti, R.; Russo, M.V. *J. Phys. Chem. C* **2012**, 116, 15795−15800.
[13] Battocchio, C.; Meneghini, C.; Fratoddi, I.; Venditti, I.; Russo, M.V.; Aquilanti, G.; Maurizio, C.; Bondino, F.; Matassa, R.; Rossi, M.; Mobilio, S.; Polzonetti, G. *J. Phys. Chem. C*, **2012**, 116, 19571–19578.
[14] Inganas, O.; Zhang, F.; Andersson, M. R. *Acc. Chem. Res.* **2009**, 42, 1713-1739.
[15] Puntoriero, F.; Nastasi, F.; Campagna, S.; Bura, T.; Ziessel, R. *Chem. Eur. J.* **2010**, 16, 8832-8845.
[16] Aly, S. M.; Ho, C.-L.; Wong, W.-Y.; Fortin, D.; Harvey, P.D. *Macromolecules*, **2009**, 42, 6902–6916.
[17] Pasquini, C.; Fratoddi, I.; Bassetti, M. *Eur. J. Org. Chem.* **2009**, 30, 5224-5231.
[18] Wan, H.; Chen, L.; Chen, J.; Zhou, H.; Zhang, D.; Liu, L. *J. Dispers. Sci. Techn.* **2008**, 29, 999-1002.
[19] Gu, T.; Whitesell, J.K.; Fox , M.A. *Chem. Mater.* **2003**, 15, 1358-1366.
[20] Shaporenko, A.; Elbing, M.; Blaszczyk, A.; von Hänisch, C.; Mayor, M.; Zharnikov, M. *J. Phys. Chem. B* **2006**, 110, 4307-4317.
[21] Haiss W, Wang C, Jitchati R, Grace I, Martín S, Batsanov AS, Higgins SJ, Bryce MR, Lambert CJ, Jensen PS, Nichols RJ. *J. Phys. Condensed Matter*, **2008**, 20, 374119
[22] Quintiliani, M.; García-Frutos, E.M.; Vázquez, P.; Torres, T. *J. Inorg. Biochem.* **2008**, 102, 388–394.
[23] Martínez-Díaz, M.V.; Quintiliani, M.; Torres, T. *Synlett* **2008**, 1, 1–20.
[24] Pearson, D. L.; Tour, J. M. *J. Org. Chem.* **1997**, 62, 1376-1387.
[25] Quintiliani, M.; Pérez-Moreno, J.; Asselberghs, I.; Vázquez, P.; Clays, K.; Torres, T. *J. Phys. Chem. B* **2010**, 114, 6309–6315.
[26] Quintiliani, M.; Kahnt, A.; Wölfle, T.; Hieringer, W.; Vázquez, P.; Görling, A.; Guldi, D.M.; Torres, T. *Chem. Eur. J.* **2008**, 14, 3765–3775.
[27] Quintiliani, M.; Kahnt, A.; Vázquez, P.; Guldi, D.M.; Torres, T. *J. Mater. Chem.*, **2008**, 18, 1542–1546.
[28] Kahnt, A.; Quintiliani, M.; Vázquez, P.; Guldi, D.M.; Torres, T. *ChemSusChem* **2008**, 1, 97–102.
[29] Gryco, D. T.; Clausen, C.; Roth, K. M.; Dontha, N.; Bocian, D. F.; Kuhr, W. G.; Lindsey, J. S. *J. Org. Chem.* **2000**, 65, 7345-7355.
[30] Shi, Z.-F.; Wang, L.-J.; Wang, H.; Cao, X.-P.; Zhang, H.-L. *Org. Lett*. **2007**, 9, 595-598.
[31] Brust, M.; Walker, M.; Bethell, D.; Schiffrin, D.J.; Whyman, R. *Chem. Commun.,* **1994**, 801-802.
[32] Vitale, F.; Mirenghi, L.; Piscopiello, E.; Pellegrini, G.; Trave, E.; Mattei, G.; Fratoddi, I.; Russo, M.V.; Tapfer, L.; Mazzoldi, P. *Mat. Sci. Engin. C*, **2007**, 27, 1300–1304.
[33] Yee, C.K.; Jordan, R.; Ulman, A.; White, H.; King, A.; Rafailovich, M.; Sokolov, J. *Langmuir*, **1999**, 15, 3486
[34] Tour, J.M.; Jones, L.; Pearson, D.L.; Lamba, J.J.S.; Burgin, T.P.; Whitesides, G.M.; Allara, D.L.; Parikh, A.N.; Atre, S.V. *J. Am. Chem. Soc.* **1995**, 117, 9529-9534.
[35] Hoestler, M.J.; Templeton, A.C.; Murray, R.W. *Langmuir* **1999**, 15, 3782-3789.
[36] Brousseau, L.C.; Novak, J.P.; Marinakos, S.M.; Feldheim, D.L. *Adv. Mater*. **1999**, 11, 447-449.
[37] Yan, H.; Lim, S.I.; Zhang, L.-C.; Gao, S.-C.; Mott, D.; Le, Y.; Loukrakpam, R.; An, D.-L.; Zhong, C.-J. *J. Mater. Chem.* **2011**, 21, 1890-1901.
[38] Brust, M.; Bethell, D.; Kiely, C.J.; Schiffrin, D.J. *Langmuir* **1998**, 14, 5425-5429.
[39] Elsevier, B.V. *J. Organomet. Chem*. **2009**, 694, 1138-1143.
[40] Parker, J. F.; Choi, J.-P.; Wang, W.; Murray, R. W. *J. Phys. Chem. C* **2008**, 112, 13976–13981.
[41] Wu, Z.; Jin, R. *Nanoletters* **2010**, 10, 2568-2573.
[42] Eustis, S.; El-Sayed, M.A. *Chem. Soc. Rev.* **2006**, 35, 209-217.
[43] Goldys, E.M.; Sobhan, M.A. *Adv. Funct. Mater*. **2012**, 22, 1906-1913.
[44] Zheng, J.; Zhang, C.; Dickson, R.M. *Phys. Rev. Lett.* **2004**, 93, 077402.
[45] Leclerc, M.; Ranger, M.; Belanger-Gariepy, F. *Acta. Cryst.* **1998**, C54, 799-801.
[46] Cametti, C.; Fratoddi, I.; Venditi, I.; Russo, M.V. *Langmuir*, **2011**, 27, 7084–7090.
[47] Scofield, J.M. *J. Electron Spectrosc. Relat. Phenom.* **1976**, 8, 129-137.
[48] NIST Standard Reference Database 20, Version 3.5 [http://srdata.nist.gov/xps/.
[49] Gryco, D. T.; Clausen, C.; Roth, K. M.; Dontha, N.; Bocian, D. F.; Kuhr, W. G.; Lindsey, J. S. *J. Org. Chem.* **2000**, 65, 7345-7355.
[50] Shi, Z.-F.; Wang, L.-J.; Wang, H.; Cao, X.-P.; Zhang, H.-L. *Org. Lett.* **2007**, 9, 595-598.